Small diameter electrospun silk fibroin vascular grafts: mechanical properties, *in vitro* biodegradability, and *in vivo* biocompatibility

Valentina Catto[a,b], Silvia Farè[a,b], Irene Cattaneo[c], Marina Figliuzzi[c], Antonio Alessandrino[d], Giuliano Freddi[d], Andrea Remuzzi[c,e], Maria Cristina Tanzi[a,b]

[a] Biomaterials Laboratory, Department of Chemistry, Materials and Chemical Engineering "G. Natta", Politecnico di Milano, Piazza L. Da Vinci 32, Milano, Italy

[b] Local Unit Politecnico di Milano, INSTM, Italy

[c] IRCCS - Istituto di Ricerche Farmacologiche Mario Negri, Bioengineering Department, via Stezzano 87, Bergamo, Italy

[d] INNOVHUB - SSI, Div. Stazione Sperimentale per la Seta, via G. Colombo 83, Milan, Italy

[e] Università di Bergamo, Industrial Engineering Department, Via Marconi 5, Dalmine, Bergamo, Italy

Corresponding author

Silvia Farè

Biomaterials Laboratory, Department of Chemistry, Materials and Chemical Engineering "G. Natta", Politecnico di Milano

P.zza L. da Vinci 32, 20133, Milano, Italy

Phone: +39-0223993389

email: silvia.fare@polimi.it

Abstract

To overcome the drawbacks of autologous grafts currently used in clinical practice, vascular tissue engineering represents an alternative approach for the replacement of small diameter vessels. With the aim of designing a suitable scaffold for this application, in the present work the production and characterization of small diameter tubular matrices (inner diameter (ID) = 4.5 and 1.5 mm), obtained by electrospinning (ES) of *Bombyx mori* silk fibroin (SF), has been considered. ES-SF tubular scaffolds with ID = 1.5 mm are original, and can be used as vascular graft in pediatrics or in hand microsurgery. Both ID 4.5 and 1.5 ES-SF tubes were successfully electrospun with a random distribution of homogeneous nanofibers with no significant differences between the two types of matrices (mean values ≅ 550 nm). Axial and circumferential tensile tests on ES-SF tubes at 37°C in wet conditions showed a higher UTS in circumferential direction than native anterior descending human coronary arteries and higher strain at break than human saphenous veins, in both directions. The suture retention strength increased with the wall thickness. The burst pressure and the compliance of ES-SF tubes were estimated using the Laplace's law. Specifically, the burst pressure was higher than the physiological pressures and the compliance was similar or higher than that of native rat aorta and Goretex® prostheses. By consequence, the mechanical properties of the developed ES-SF tubes resulted appropriate for small diameter blood vessel regeneration. Enzymatic *in vitro* degradation tests demonstrated a decrease of the order and crystallinity of the external SF layer as a consequence of the enzyme (i.e. Protease type XIV) activity, which attacked the nanofibers from the outside, producing a 35% weight loss after 24 days. The *in vitro* cytocompatibility of the ES-SF tubes was confirmed by the adhesion and growth of primary porcine smooth muscle cells. The *in vivo* subcutaneous implant into the rat dorsal tissue indicated that electrospun fibroin matrices caused a mild host reaction, by promoting a limited fibrotic reaction. The results of this work, which to the best of our knowledge for the first time comprehensively evaluated morphological and mechanical aspects of ES-SF tubular scaffolds, their *in vitro* degradation and *in vitro* and *in vivo* biocompatibility, suggest the potential suitability of these matrices as scaffolds for the regeneration of small diameter blood vessels.

Keywords

Silk fibroin; electrospinning; small diameter vascular grafts; mechanical properties; *in vitro* degradation; *in vitro* and *in vivo* biocompatibility

1.Introduction

Due to the increase of both peripheral arterial occlusive diseases and coronary heart diseases, every year there is a strong patient demand for small diameter vascular grafts (internal diameter (ID) < 6 mm). Although synthetic polymeric materials (i.e. Dacron®, Goretex®) have been successfully used for large and medium diameter vessels (ID ≥ 6 mm), they fail at smaller diameters (ID < 6 mm), due to thrombosis, anastomotic intimal hyperplasia, aneurysm formation, infection, and compliance mismatches [1-3]. To date, autologous vessels (e.g. saphenous vein or internal mammary artery) remain the clinical gold standard for small diameter vessel replacement, despite their scarce availability [1-3]. For these reasons, vascular tissue engineering represents a possible innovative approach, developing functional alternative solutions.

The design requirements of an ideal small diameter vascular graft are stringent and mainly regard biocompatibility and appropriate mechanical properties. Specifically, tissue engineered vascular grafts should be non-toxic, biocompatible and non-thrombogenic [3-5]. Furthermore they should be able to support the variation in blood pressure and the blood flow without outflows, due to appropriate structure and suitable mechanical properties in terms of compliance, burst pressure, strength and suture retention [3-5]. After *in situ* implantation, tissue engineered vascular grafts should remodel into a functional blood vessel, in particular they should promote the complete regeneration of the endothelium [3-5]. Tissue engineered vascular grafts have been developed using decellularized matrices (such as porcine abdominal aorta and carotid [6], human umbilical artery [7]), biodegradable synthetic polymers (such as polyglycerol sebacate (PGS) [8], poly-ε-caprolactone (PCL) [9, 10]) or natural polymers (such as recombinant human tropoelastin [11], fibrin [12], silk fibroin [5]) [3, 4]. To attract cells into the vessel graft, natural polymers are studied and used for the scaffold fabrication due to their similarity with human tissues. Among them, silk fibroin appears very promising for its peculiar properties. Silks are spun into fibers by some lepidopters or spiders and, depending on the source, have specific composition, structure and properties [13]. Silk from the silkworm *Bombyx mori* is the most extensively used and characterized for biomedical application [13]. *Bombyx mori* silk fibers are composed of two filaments of the protein fibroin, coated by a glue-like protein, sericin [13-15], that was identified as a possible source of non physiological inflammatory reaction, and therefore usually removed by a degumming process [13-15]. Silk fibroin (SF), after degumming, presents high biocompatibility, excellent mechanical properties, and versatile processability.

Consequently, SF has emerged as an attractive biomaterial for producing scaffolds for several applications in tissue engineering [13, 15].

One of the key elements of tissue engineering is typically the production of ideal scaffolds able to mimic the native structure of the extracellular matrix (ECM), promoting the repopulation of the scaffold by host cells and the production of a new natural ECM. Following a biomimetic approach, nanofibrous scaffolds (made of fibers with diameters between 1 and 1000 nm) are widely used for tissue engineering applications due to the similarity with the size of native ECM fibers [16-18]. The most common methods used for nanofiber production are self-assembly, phase separation and electrospinning [1, 16]. Among these techniques, electrospinning (ES) is the simplest and the most efficient process; in addition, it is a versatile method that is able to produce continuous fibers, ranging from few nanometer to some micrometers, using several materials (polymers, blends of polymers, polymers loaded with other materials or additives such as inorganic particles, growth factors, other biomolecules and living cells [17]) [4, 16-18]. Furthermore, electrospun scaffolds are characterized by a high surface to volume ratio, that provides a large surface area for cell attachment [16-18].

In the present work, we describe the design, production and characterization of tubes with 4.5 and 1.5 mm inner diameters made of electrospun silk fibroin (ES-SF). Electrospun scaffolds with ID $\leq$ 1.5 mm made of PCL [19], a copolymer of ε-caprolactone and L-lactide (PCL/PLA) [20], and blends of PCL and poly-D,L-lactide (PDLLA) [21] are reported in literature, and silk fibroin was already evaluated for the fabrication of small diameter blood vessel grafts [5, 22, 23], including electrospun tubular matrices [24-28]. However, to the best of our knowledge, this is the first work which has extensively evaluated ES-SF tubes, considering morphological and mechanical aspects, *in vitro* degradation, and *in vitro* and *in vivo* biocompatibility. ES-SF tubular scaffolds with such a small diameter (ID = 1.5 mm) are novel SF biomaterial scaffolds, not yet reported in literature, as they were obtained by electrospinning of SF in tubular shape without any other material . They can be used as vascular grafts in pediatrics or in hand microsurgery.

2.Materials and methods

2.1.Materials

Bombyx mori cocoons were kindly supplied by the CRA (Council of Research and Experiments in Agriculture, Apiculture and Sericulture Unit, Padua, Italy). All chemical reagents were obtained from Sigma Aldrich, unless mentioned otherwise.

2.2.Preparation of regenerated *Bombyx mori* silk fibroin films

SF films, required for the preparation of the solution for the electrospinning process, were prepared as follows. The *Bombyx mori* cocoons were degummed in autoclave at 120°C for 15 min and then rinsed with distilled water to extract sericin. After drying at room temperature and storing under controlled conditions (T = 20 ± 2°C, r.h. = 65 ± 2%), the extracted SF fibers were neutralized to reach the isoelectric point (pI) of SF heavy-chain (pI = 4.2 [29]). Briefly, SF fibers were soaked in an aqueous solution of 0.05 M sodium bicarbonate and 1g/l sodium dodecyl sulfate for 30 min. Then, SF fibers were immersed in an aqueous solution of 0.01 M acetic acid and 0.01 M sodium acetate (0.01 M AA + 0.01 M NaA) for 30 min. Subsequently, SF fibers were soaked again in a 0.01 M AA + 0.01 M NaA for at least 14 h, and finally rinsed with distilled water for 30 min. After drying at room temperature and storing under controlled conditions as above described, SF fibers were solubilized in a 9.3 M lithium bromide (LiBr) aqueous solution (T = 60 ± 2°C, t = 3 h) to obtain a 10% w/v SF solution. The solution was then diluted with distilled water to obtain a 2% w/v SF concentration, and dialyzed against distilled water for 3 days using cellulose membrane dialysis tubing (molecular weight cut-off = 12,000), to eliminate LiBr salts. SF films were prepared by pouring 15 ml of the 2% w/v SF solution into Petri dishes (∅ = 5.5 cm), followed by casting under fume hood at room temperature until complete solvent evaporation.

2.3.Electrospinning of silk fibroin tubes

A 7.5 % w/v SF solution was prepared at room temperature by dissolving SF films in formic acid (98 vol. %) and electrospun with a home-made electrospinning (ES) apparatus. The SF solution was placed in a 10 ml polypropylene syringe and forced by a syringe-pump (KD Scientific, KDS 100), at 1.1 ml/h constant volume flow rate, into the spinneret, a stainless steel capillary tube (ID = 1.1 mm). The spinneret was connected to the positive output (+12 kV) of a high voltage power supply (Fug Elektronik GmbH, HCN 35-12500), while the negative pole (-12 kV) was joined to the fiber collector, to obtain an electric potential difference of 24 kV. The spinneret was moved horizontally by a DC-motor (RS Components) equipped with a linear guide (RS Components) to allow a more uniform fiber deposition onto the collector. ES-SF tubular scaffolds were prepared using stainless steel mandrels, as rotating collectors (~ 2700 rpm), that were placed at 10 cm from the spinneret. ES-SF 4.5 ID and ES-SF 1.5 ID tubes were fabricated using collectors with 4.5 and 1.5 mm diameters,

respectively. To facilitate the removal of ES-SF tubes from the mandrels, a sacrificial layer of PEO (200,000 Da) was electrospun on the mandrels before the SF deposition. Briefly, an aqueous PEO solution (7.5% w/v) was electrospun onto the rotating mandrel, placed at 10 cm from the spinneret, using a flow rate and a potential difference equal to 1.1 ml/h and 24 kV, respectively. After overnight drying, SF solution was electrospun onto the mandrels coated with PEO. After the complete evaporation of formic acid, ES-SF tubular scaffolds (ES-SF 4.5 ID and ES-SF 1.5 ID) were treated with methanol (> 99.9%) for 15 min to induce SF crystallization and partially dissolve PEO, facilitating the ES-SF tube removal from the collectors. Finally, ES-SF tubular scaffolds were rinsed with distilled water at 37°C for 48 h, before further characterization.

2.4.Morphological characterization

The wall thickness of the ES-SF tubular scaffolds was measured with a micrometer in three different points for each specimen (n = 3 for each ID). The morphology of the two types of ES-SF tubular scaffolds was observed by Scanning Electron Microscopy (SEM, Cambridge Instrument Stereoscan 360). The specimens were mounted onto aluminum stubs, gold sputter-coated (Edwards Sputter Coater 5150B) and observed at different magnifications with a 10 kV accelerating voltage. The average fiber diameter was determined from SEM images (5000x) using ImageJ software (US National Institute of Health), by analyzing 100 electrospun fibers.

2.5.Axial and circumferential tensile tests

Axial and circumferential tensile tests were performed on ES-SF 4.5 ID and ES-SF 1.5 ID tubular samples, using a dynamic mechanical analyzer (DMA Q800, TA Instruments).

For axial tensile tests, tubular specimens (n = 3 for each ID tubular scaffold, length = 17 mm, gauge length = 8 mm) were cut by a scalpel from different ES-SF tubular scaffolds. Samples were imbibed in phosphate buffered saline (PBS) for 10 min and tested at 37°C with a preload of 0.005 N and a force ramp of 0.05 N/min until break.

Circumferential tensile tests were performed using home-made ad hoc grips (Fig. 1 A). For each kind of tubular scaffold, ring-shaped specimens (n = 3 for each ID, axial length = 4 mm) were cut by a scalpel from different ES-SF tubes, imbibed in PBS for 10 min, and tested at 37°C with a preload of 0.01 N and a force ramp of 0.05 N/min until break.

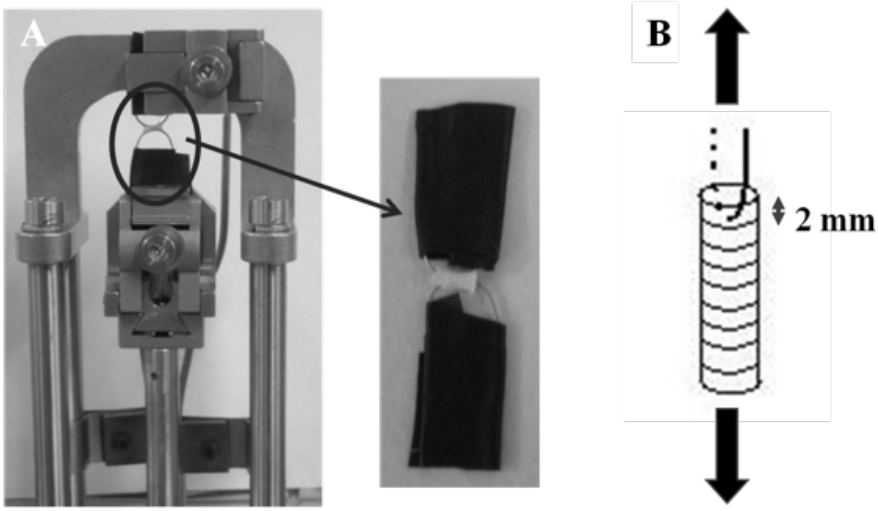

Fig. 1. (A) Custom clamps for circumferential tensile tests. (B) Sketch of the set-up for suture retention strength tests.

The following mechanical parameters were drawn from the obtained stress/strain curves: elastic modulus (E), ultimate tensile strength (UTS), and strain at break (ε_b). UTS and ε_b were considered the maximum stress value before failure and its corresponding value of strain, respectively. The elastic modulus was calculated using a least-square fitting in the range of 0-25% strain and in the range of 0-8% for axial and circumferential tensile tests, respectively. In addition, for circumferential tensile tests, the curve slope was measured in a second range of strain (8 – 25%).

2.6.Estimated burst pressure

In accordance to Gauvin et al. [30], the estimated burst pressure (BP) was calculated by rearranging the Laplace's law for a pressurized thin-walled hollow cylinder:

$$BP_{estimated} = 2\frac{UTS \cdot t}{ID} \qquad (1)$$

where UTS was measured by circumferential tensile tests, t is the wall thickness and ID is the unpressurized inner diameter of the ES tubular scaffolds. A graft is defined as thin-walled hollow cylinder when the ratio between its thickness and its diameter is minor than 0.1; therefore, referring to the morphological analysis, ES-SF 4.5 ID and ES-SF 1.5 ID tubular scaffolds can be considered thin-walled hollow cylinders.

2.7 Estimation of tubular scaffold distensibility and compliance

In accordance to Benetos et al. [31], the effect of the distension on the stretching of an artery wall can be evaluated using the distensibility coefficient (DC), defined as:

$$DC = 2\frac{D_s - D_d / D_d}{\Delta P} \qquad (2)$$

where Ds is the systolic diameter, Dd is the diastolic diameter and ΔP is the pulse pressure (systolic minus diastolic blood pressure). This parameter represents the strain of the arterial wall for a given pressure and pertains to the mechanical loading of the artery during a cardiac cycle. In this work, we considered the DC for a preliminary estimation of the ES-SF tubular scaffold compliance in the physiological pressure range (80 mmHg – 120 mmHg). To calculate the DC, the Laplace's law and the load/displacement curves obtained by circumferential tensile tests were used. The Laplace's law for a pressurized thin-walled hollow cylinder is equal to:

$$\sigma_c = P\frac{ID}{2 \cdot t} \qquad (3)$$

where σ_c is the wall stress, P is the considered pressure (80 and 120 mmHg), ID is the inner diameter of the ES tubular scaffolds and t is the wall thickness. The estimated DC of native rat abdominal aorta, harvested from a male Sprague Dawley rat (rat weight = 300 g), and of a Goretex® prosthesis (ID = 3.5 mm) were considered as control.

2.8 Determination of suture retention strength

Suture retention strength tests were performed to determine the force necessary to pull a suture from the tubular graft or cause the wall of the graft to fail. In accordance with the standard practice ISO 7198 "Cardiovascular implants – Tubular vascular prostheses", a suture (8-0 Prolene, Ethicon) was inserted at a distance of 2 mm from the edge of the ES-SF 1.5 ID tubular specimens (length = 15 mm) through the tube wall to form a half loop (Fig. 1 B). The 8-0 Prolene suture had the same size of one used for *in vivo* implants of gel spun SF tubes into the rat abdominal aorta (8–0 monofilament Polypropylene suture) [5]. As the only parameter that should influence the suture retention strength of the graft is the wall thickness, we performed the test only on ES-SF 1.5 ID tubes. ES-SF 1.5 ID tubular scaffolds were purposely produced with different wall thickness (ES-SF 1.5A = 40 ± 10 μm, ES-SF 1.5B = 80 ± 15 μm, ES-SF 1.5C = 120 ± 25 μm) to investigate the influence of this parameter on the suture retention strength. Specimens (n = 3 for each considered wall thickness) were imbibed

in PBS for 10 min before tests. The suture and the opposite edge of the tubular specimen were fixed in the clamps of a MTS 1M/H apparatus. Tests were performed at a cross-head displacement rate of 50 mm/min up to pull the suture through the tubular sample or cause the sample wall to break (ISO 7198). Mean and standard deviation values of suture retention strength were calculated for each investigated wall thickness.

2.9 Enzymatic degradation tests

Tubular specimens (~5 mg in weight) were cut by a scalpel from the ES-SF 4.5 ID tubular scaffolds. The larger tube diameter was chosen for this test because of the higher exposed surface, available to the enzyme. After 12 h at 20°C and 60% relative humidity, the specimens were weighed and then sterilized in autoclave at 120°C for 15 minutes. A 1 U/ml enzymatic solution of Protease Type XIV from *Streptomyces griseus* was prepared in a buffered solution containing 10 mM sodium acetate and 5 mM calcium acetate (pH 7.5) [32], and sterilized by filtration. Specimens of ES-SF tubes were incubated at 37°C in protease solution at an enzyme concentration of 0.1 U/mg or in buffer solution (blank). The tests were carried out in triplicate for each time point; enzymatic and buffer solutions were renewed every 3 days. At predetermined time-points (t = 1, 2, 3, 4, 7, 10, 17, 24 days), the specimens were removed from the solutions, treated with hot distilled water (T = 80°C) for 30 min to inactivate the enzyme (only for the samples extracted from enzymatic solution), rinsed at room temperature in distilled water to remove residuals of salts, and dried overnight at 20°C and 60% r. h. before further analysis. The weight variation (ΔW %) of the ES-SF samples, after incubation in enzymatic or buffered solution, was calculated at each time-point according to the formula (1):

$$\Delta W\% = \frac{(W_0 - W_t)}{W_0} \times 100 \qquad (4)$$

where W_0 is the weight at t = 0, and W_t the weight at the time-point t.

The morphology of ES-SF specimens was evaluated by SEM (Jeol JSM-6380 LV). The samples were mounted onto aluminum stubs, gold sputter-coated (Automatic Sputter Coater, Gressington 108 Auto) and observed at different magnifications with a 20 kV accelerating voltage. Crystallinity variation of the ES-SF samples was studied by Fourier transform infrared spectroscopy (FTIR) with a Thermo Nicolet 6700 FT-IR spectrometer, equipped with an attenuated total reflectance (ATR) accessory and ZnSe crystal. Spectra were normalized to the 1446 cm^{-1} peak before any data processing. The FTIR Crystallinity Index (CI) was calculated as the intensity ratio between the amide III bands at 1260 cm^{-1} and 1230

cm^{-1} (I_{1260}/I_{1230}) [25, 33]. Differential Scanning Calorimetry (DSC) analyses were performed with a Q200 DSC (TA Instruments) using standard aluminum pans. Specimens of about 2-4 mg were heated from 20 up to 500°C, under N_2 atmosphere, at a 10°C/min scanning rate. Specifically, the variation of the melting/decomposition peak values, calculated from the DSC thermograms, were assessed during the incubation time. The samples were analyzed in duplicate.

2.10 *In vitro* cell interaction study

Primary porcine aortic SMCs were isolated from pigs as previously described [34] and used at passage 4. Briefly, SMCs were isolated from normal 2-4 week-old pigs by a collagenase digestion [34]. The SMCs were cultured in Dulbecco's modified Eagle's medium (DMEM), containing 4.5g/L glucose (DMEM high glucose) supplemented with 10% fetal bovine serum (FBS, Lonza), 10% porcine serum (Euroclone), 4 mM L-glutamine (Life Technologies), 1% penicillin/streptomycin solution (Life Technologies), 5 mM N-2-hydroxyethylpiperazine-N-2-ethanesulfonic acid (HEPES). For cell expansion, the medium was replaced three-times a week and the cultures were maintained in a humidified incubator at 37°C and 5% CO_2.

ES-SF 1.5 ID tubular samples (length = 1 cm, n = 3 for each time-point), previously ethylene oxide sterilized, were seeded at a density of 1x106 cells per sample using a rotating device (Stuart Rotator SB3). The cell suspension (2 ml) was placed in a cryovial and each ES-SF 1.5 ID sample mounted onto a mandrel was put inside the vial. Cryovials rotated for 4 h in a humidified incubator to promote cell adhesion on the tubular scaffolds. The ES-SF 1.5 ID scaffolds were then statically cultured in 15 ml culture medium, that was replaced every 2 days, for 7 days.

After 3 and 7 days of culture, cell distribution onto ES-SF 1.5 ID tubular scaffolds was evaluated by 3-[4,5-dimethylthiazol-2]- 2,5-dipheniltetrazolium bromide (MTT) assay. Cell seeded samples were rinsed with PBS (Invitrogen) and incubated for 3 h at 37°C with 0.5 mg/ml MTT in sterile DMEM medium without phenol red. After incubation, unreacted MTT was removed by rinsing with PBS. Finally, ES-SF samples were observed with an optical microscope (Carl Zeiss) to qualitatively analyze the cell distribution on their surface.

After 7 days of culture, the ES-SF 1.5 ID tubular scaffolds were fixed in Bouin's solution (Diapath) for 4h at 4°C, dehydrated in ascending concentrations of alcohol and embedded in paraffin. Sections (3µm thick) of ES-SF1.5 ID samples were stained with hematoxylin and eosin (H&E) and observed with an optical microscope (Carl Zeiss) to analyze the cell distribution in the tube cross-section.

2.11 *In vivo* subcutaneous implantation

Three male Lewis rats weighting 200-250 g were used for *in vivo* subcutaneous tests. The animals were maintained under standard conditions (12 h light: dark cycle, controlled room temperature at 20 - 22°C, r. h. > 60%) and housed individually with free access to standard pellet diet and water. Animal care and treatment, anesthesia and sacrifices at the end of the trial were conducted in accordance with institutional guidelines that are in compliance with national (n.116, suppl. 40, 18 febbraio 1992, Circolare n.8, 14 luglio 1994) and international (EEC Council Directive 86/609, OJL358-1, Dec. 1987; Guide for the Care and Use of Laboratory Animals, U.S. National Research Council, 1996) guidelines and policies. Ethylene oxide sterilized flat ES-SF specimens (10 x 10mm), cut from different ES-SF 4.5 ID tubes, were implanted in the dorsal subcutaneous tissue of the rats (Fig. 2 A). Each sample was fixed to the tissue with a 4.0 silk suture (Ethicon Inc.) to maintain the sample on site. After 15 days the animals were euthanized by CO_2 inhalation and the grafts were harvested.

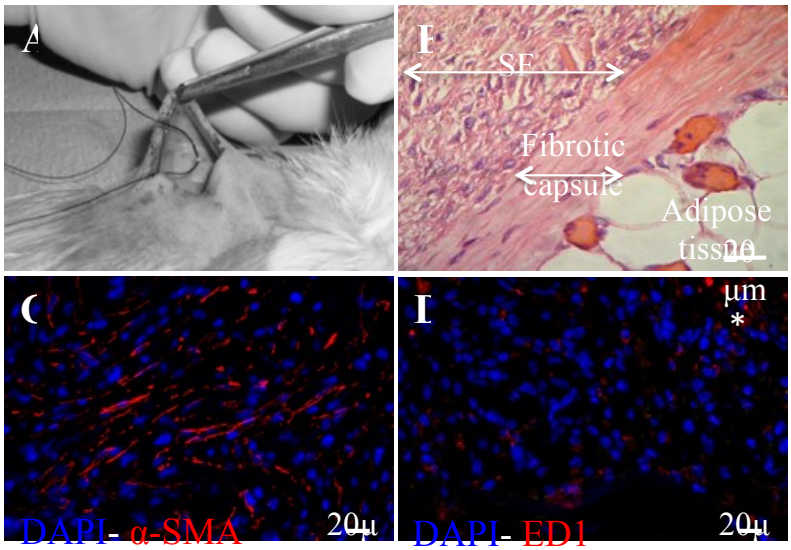

Fig. 2. (A) ES-SF tubular scaffolds implanted subcutaneously in Lewis male rats for 15 days. (B) Histological image by H&E staining of ES-SF samples 15 days after implantation. (C) Immunofluorescence analysis of fibroblasts (red) and (D) of macrophages (*, red) and T lymphocytes (green); magnification 40x.

Immediately after the explant, the samples were washed in 0.9% NaCl, immersed for fixation in Bouin's solution (BioOptica) overnight, subsequently dehydrated in graded ethanol series and cleared in toluene (BioOptica), before paraffin embedding. Microtome sections (5 µm

thick) were processed and stained for light microscopy studies. H&E staining was used to assess the tissue integration of the material in the host tissue. The stained sections were observed under a light microscope fitted with a digital camera (Olympus).

Immunofluorescence staining was performed to evaluate the presence of host fibroblasts in explanted fibroin and the inflammatory response induced *in vivo* by the ES-SF samples. Briefly, explanted samples were fixed overnight with 4% paraformaldehyde in PBS and frozen in liquid nitrogen. Slides of frozen tissue were incubated with anti actin-α-smooth muscle-Cy3 for fibroblast characterization. For macrophages and T lymphocytes, slides were incubated with primary antibody mouse anti-rat ED1 (Chemicon Int) and goat anti-human CD4 (Santa Cruz Biotechnology, Inc.), respectively. They were then incubated with secondary antibody donkey anti-mouse Cy3 or rabbit anti-goat Cy2 (Jackson ImmunoResearch) for macrophages and T lymphocytes, respectively. Counter staining with DAPI (1 μg/ml) was performed for cell nuclear staining. Stained samples were finally examined by laser confocal microscopy (LSM 510 Meta, Carl Zeiss) at excitation/emission wavelengths of 550/570 nm and 492/510 nm for detecting Cy3 and Cy2, respectively.

2.12 Statistical analysis

Data, where possible, were expressed as mean ± standard deviation and statistically compared by two-sample t-Test (significance level = 0.05), Origin® Pro v. 8.5 software. Suture retention strength of each investigated wall thickness was statistically compared by One-way ANOVA (significance level = 0.05 and Tukey means comparison), Origin® Pro v. 8.5 software.

3. Results

3.1 Morphological characterization

Nanostructured ES-SF tubular scaffolds were successfully produced with 4.5 and 1.5 mm ID (Fig. 3 A and B). The wall thickness was 104 ± 14 μm and 44 ± 7 μm, for ES-SF 4.5 ID and ES-SF 1.5 ID, respectively. SEM analyses showed a homogeneous random fiber distribution, with fiber diameters in the nanometric range (Fig. 3 C and D). Specifically, the average fiber diameter was 547 ± 132 nm and 555 ± 155 nm for ES-SF 4.5 ID and ES-SF 1.5 ID scaffolds, respectively. The fiber size was not significantly different for the two types of scaffolds. Fiber diameter distributions of ES-SF 4.5 ID and ES-SF 1.5 ID tubes are shown in Fig. 3 E and F, respectively. The fiber diameters ranged from 350 to 1270 nm for ES-SF 4.5 ID and

from 350 to 990 nm for ES-SF 1.5 ID tubes, respectively, with a narrower diameter distribution for 4.5 ID ES samples.

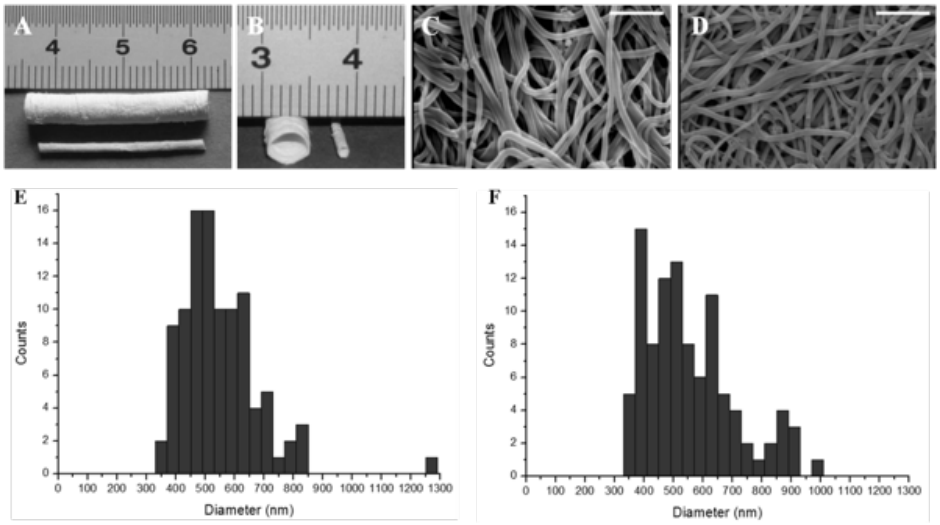

Fig. 3. Macrographs of the length (A) and of the diameter (B) of ES-SF 4.5 ID and ES-SF 1.5 ID tubes. SEM images of ES-SF 4.5 ID (C) and SEM image of ES-SF 1.5 ID (D) tubes (scale bars: 5 μm). Fiber diameter distribution of ES-SF 4.5 ID (E) and ES-SF 1.5 ID (F) tubes.

3.2 Mechanical characterization

Tensile axial and circumferential tests

Representative stress-strain curves obtained by tensile axial mechanical tests showed a similar behavior for both ES-SF tubes (Fig. 4 A). Two different zones can be detected in the stress/strain curves (Fig. 4 A): in the first zone (ε = 0 - 25%), a higher elastic modulus (i.e. higher curve slope) is probably due to the presence of numerous sticking points at fiber crossovers, which resist to the applied force, limiting fiber rearrangement in the direction of the applied force; in the second zone (ε > 25%), the decrease in curve slope could be associated to the break of the sticking points at crossovers, to an easier extension of nanofibers in the force direction, as well as to the breaking of nanofibers themselves. Comparing ES-SF 4.5 ID with ES-SF 1.5 ID samples (Table 1), only the values of elastic modulus were significantly different ($p < 0.05$).

Table 1. Mean and standard deviation values of the considered mechanical parameters obtained by axial and circumferential tensile tests for ES-SF 4.5 ID and ES-SF 1.5 ID scaffolds. (*) = $p<0.05$.

		ES-SF 4.5 ID	ES-SF 1.5 ID
Axial tensile test	**Elastic modulus [MPa] (*)**	0.61 ± 0.15	1.33 ± 0.37
	Ultimate tensile strength [MPa]	0.83 ± 0.13	0.95 ± 0.09
	Strain at break [%]	224 ± 29	199 ± 16
Circumferential tensile test	**Elastic modulus (ε = 0 – 8 %) [MPa]**	0.55 ± 0.01	0.43 ± 0.10
	Stiffness (ε = 8 – 25 %) [MPa] (*)	1.37 ± 0.04	0.41 ± 0.11
	Ultimate tensile strength [MPa] (*)	1.24 ± 0.06	0.90 ± 0.07
	Strain at break [%](*)	141 ± 19	210 ± 33

Representative stress-strain curves obtained by tensile circumferential mechanical tests exhibited a different behavior, depending on ES-SF tube diameter, specifically in the last part ($\varepsilon > 60\%$) of the stress-strain curves (Fig. 4 B). In the first part ($\varepsilon < 8\%$, low-strain regime), a similar linear elastic behavior was detected for ES-SF 4.5 ID and ES-SF 1.5 ID, as confirmed by the elastic modulus values ($p > 0.05$, Table 1). In the second range of strain (8% – 25%), ES-SF 4.5 ID showed a higher curve slope, hence a higher stiffness, than ES-SF 1.5 ID ($p < 0.05$, Table 1). Specifically, the slope of σ/ε curves for ES-SF 1.5 ID remained similar between ε values = 0 – 25% ($p > 0.05$, Table 1); in contrast, ES-SF 4.5 ID samples exhibited a significant change of the σ/ε slope ($p < 0.05$, Table 1). Probably, in the first range of the curves, the nanofibers partially aligned in the direction of the load, but the presence of numerous sticking points at fiber crossovers of ES-SF 4.5 ID tubes limited the fiber rearrangement, leading to a higher curve slope in the second range (Fig. 4 B, ES-SF 4.5 ID). Then, in the last part of theσ/ε curves ($\varepsilon > 60\%$), there was a decrease of slope, most likely due to the complete fiber alignment in the force direction and to the nanofiber break (Fig. 4 B). Comparing the two ES-SF tubes, strain at break, ultimate tensile strength and stiffness (in the zone of ε values between 8 and 25%) were significantly different ($p < 0.05$, Table 1).

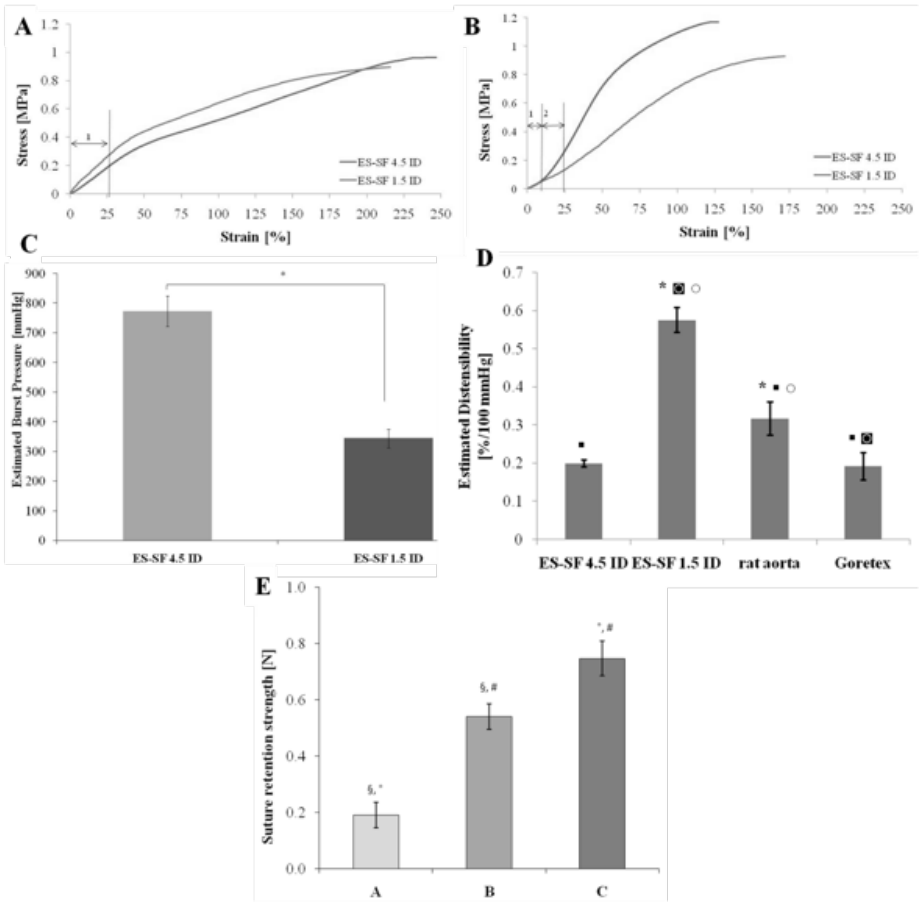

Fig. 4. (A): Representative tensile stress-strain curves of the ES-SF tubular scaffolds obtained by axial tests; the range for the detection of elastic modulus is reported. (B): Representative tensile stress-strain curves of the ES-SF tubular scaffolds obtained by circumferential tests. 1 and 2 indicate the zones considered for detection of elastic modulus and stiffness. (C): Estimated burst pressure evaluated for ES-SF 1.5 ID and ES-SF 4.5 ID tubular scaffolds. (D): Distensibility coefficient (DC) considered for a preliminary estimation of the compliance, evaluated for ES-SF 1.5 ID and ES-SF 4.5 ID tubular scaffolds, rat aorta and Goretex® prosthesis; $p < 0.05$ * relative to ES-SF 4.5 ID tubes, ▪ relative to ES-SF 1.5 ID tubes, ◙ relative to rat aorta, ○ relative to Goretex prosthesis. (E): Suture retention strength measured for the ES-SF 1.5 ID samples with different wall thickness; §, °, # statistical significance ($p < 0.05$) between A and B, A and C, B and C, respectively.

Estimation of burst pressure

The burst pressure was estimated from the stress/strain curves obtained in the tensile circumferential tests. A significant difference ($p < 0.05$, Fig. 4 C) was observed in the burst pressure of ES-SF 4.5 ID (773 ± 51 mmHg) compared to ES-SF 1.5 ID (344 ± 32 mmHg), being higher for the first one.

Estimation of distensibility

The compliance was estimated by the distensibility coefficient (DC); in particular, DC of rat aorta was higher than that of Goretex® prosthesis, while the DC value of ES-SF 4.5 ID tubes was lower than that of ES-SF 1.5 ID tubes ($p < 0.05$, Fig. 4 D), that showed the highest DC value ($p < 0.05$, Fig. 4 D).

Suture retention strength

As expected, the suture retention strength increased by increasing the wall thickness of the ES-SF 1.5 ID scaffold (Fig. 4 E). The difference of the retention strength values was significant ($p < 0.05$) among all the considered samples.

3.3 Enzymatic degradation tests

The degradation rate of ES-SF tubular scaffolds incubated with protease followed a linear trend during all the test time; the weight loss at the end of the test ($t = 24$ days) was about 35% of the initial weight (Fig. 5 A). As expected, the blank ES-SF samples, incubated only in buffer solution, did not show any weight variation (Fig. 5 A).

After 3, 7 and 17 days of incubation, SEM images (Fig. 5 B (a), (b), (c)) showed an increase in surface roughness and the appearance of cracks in the electrospun nanofibers of the ES-SF tubular scaffolds, by increasing the incubation time in the enzymatic solution. On the other hand, the blank sample incubated up to 17 days in buffer solution only (Fig. 5 B (d) still revealed well defined and smooth fibers with no sign of surface degradation.

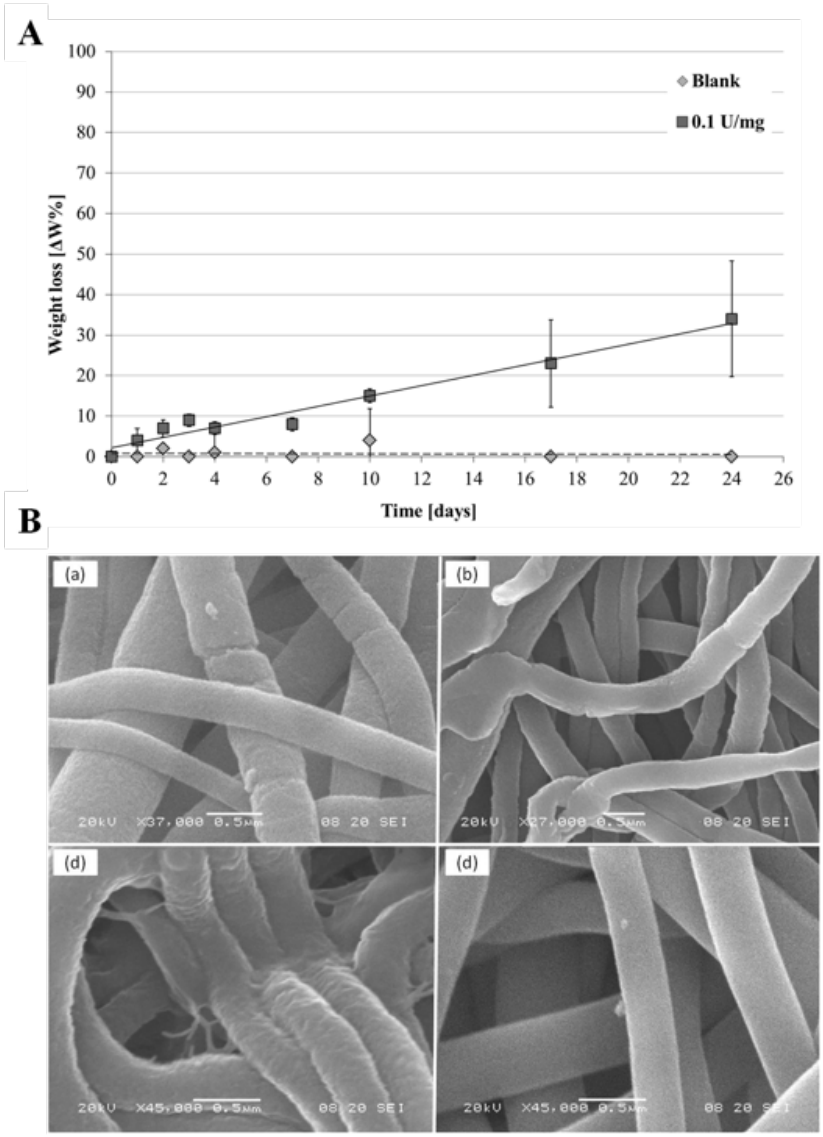

Fig. 5. (A): Percentage of weight loss of ES-SF tubes incubated in the enzyme (protease XIV) solution at 37°C; blank: ES-SF samples incubated in buffer solution. (B): SEM images of ES-SF tubes incubated in the protease XIV solution at 37°C after 3 days (a), 7 days (b), 17 days (c), blank sample after 17 days of incubation in buffer solution (d) (scale bar: 0.5 μm).

FTIR-ATR analysis assessed the possible changes in surface structure and molecular conformation of SF as a function of the degradation time for ES-SF samples treated with the

enzymatic solution, compared to the blank (after 17 days of incubation) and untreated samples. The untreated samples were not incubated in enzymatic or buffer solutions.

The FTIR spectra reported in Fig. 6 A indicate that all ES-SF samples maintained the typical β-sheet structure of untreated SF nanofibers, independently from the incubation time and the presence or not of the protease. This is confirmed by the presence of the typical β-sheet bands of the amide I (1699 cm^{-1} and 1626 cm^{-1}), amide II (1518 cm^{-1}), and amide III (1260 cm^{-1} and 1230 cm^{-1}).

To investigate possible crystallinity changes at the surface of ES-SF tubular scaffolds, the Crystallinity Index ($CI = I_{1230/1260}$) was calculated and plotted as a function of the degradation time (Fig. 6 B). Both blank and degraded samples displayed a sharp increase of the CI value after 1 and 2 days of incubation in buffer and enzymatic solutions, respectively. Afterwards, the CI of blank samples remained constant ($p > 0.05$), in contrast the CI of samples exposed to protease displayed an exponential decay ($p < 0.05$).

Bulk structural properties of ES-SF tubes incubated in buffer and enzymatic solutions were investigated by DSC analysis (Fig. 6 C). The strong melting/decomposition endotherm peak at 285.8°C in untreated SF nanofibers, is typical of regenerated SF materials with β-sheet structure [35]. By increasing the degradation time, the endotherm peak shifted to higher temperature and became sharper (Fig. 6 C), thus indicating a more ordered arrangement of the SF chains in the bulk of the material upon immersion in protease solution (Fig. 6 C). An initial sharp increase of peak temperature was detected for both blank and protease degraded samples (Fig. 6 D). Then, a plateau was attained at lower temperature for blank samples and at higher values for the protease treated samples, probably due to the enzymatic cleavage of less ordered SF domains (Fig. 6 D).

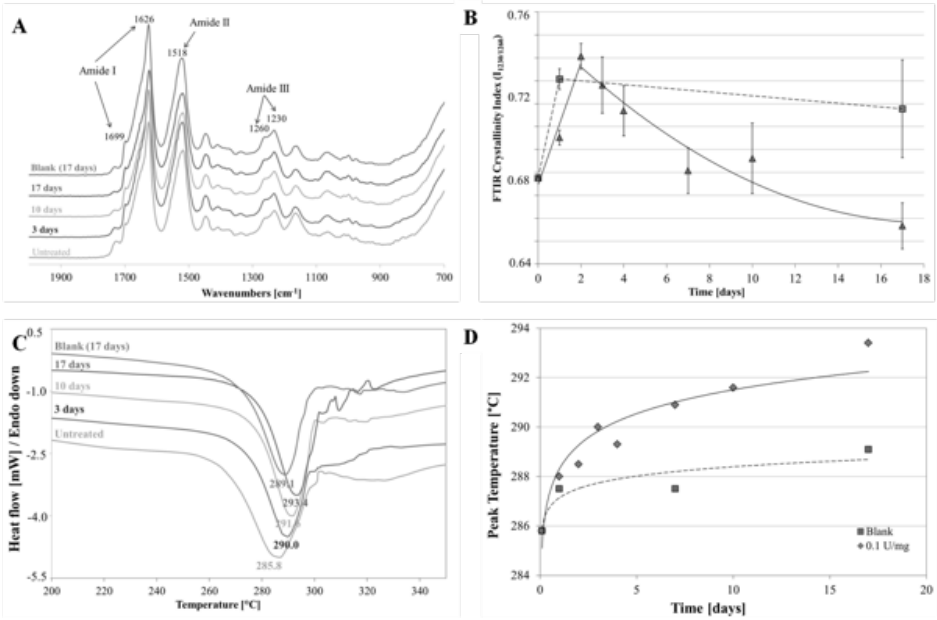

Fig. 6. (A): ATR-FTIR spectra of ES-SF tubes incubated in the protease solution at 37°C for 3, 10, and 17 days; the blank sample at 17 days was incubated in buffer solution; spectra were compared to the one of untreated ES-SF tubular scaffold. (B): Time dependence of the FTIR Crystallinity Index of ES-SF tubes incubated in the protease solution at 37°C. (C): DSC thermograms of ES-SF tubes incubated in the protease solution at 37°C for 3, 10, and 17 days; the blank sample at 17 days was incubated in buffer solution; thermograms were compared to the one of untreated ES-SF tubular scaffold. (D): Time dependence of the temperature of the melting/decomposition peak of ES-SF tubes incubated in the protease solution at 37°C. Blank refers to samples incubated in buffer solution.

3.4 *In vitro* cell interaction study

MTT assay demonstrated a homogenous SMC distribution after 3 days and 7 days, as reported in Fig. 7 A and B.

H&E staining confirmed the qualitative results obtained by the MTT assay; ES-SF 1.5 ID tubes showed a homogenous cell distribution on the outer surface, with the presence of a thin cell layer (Fig. 7 C). Furthermore, there were some cells in the tube wall thickness (Fig. 7D and E). Cells were able to migrate from the tube outer surface to the lumen, however the cell distribution into the tube thickness was heterogeneous (Fig. 7 D and E).

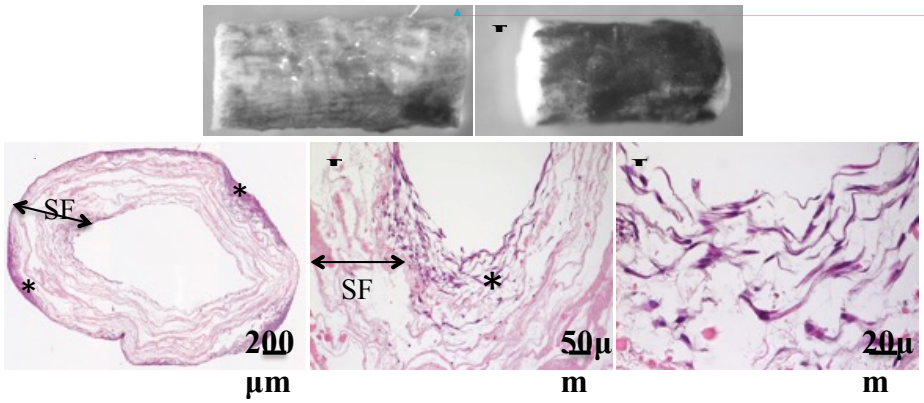

Fig. 7. Qualitative images of MTT assay performed on seeded ES-SF tubes after 3 days (A),and after 7 days (B). (C, D, E): H&E performed on seeded ES-SF 1.5 ID tubes after 7 days; (C) cross section of fibroin construct (original magnification 10x). (D and E) High magnification of cells on the inner lumen of the prosthesis (original magnification 20x and 63x). Asterisks indicate the presence of SMC

3.5 *In vivo* subcutaneous implantation

Histological analysis, performed by H&E staining on ES-SF 4.5 ID samples, explanted from the subcutaneous dorsal tissue of Lewis rats at 15 days after implantation, demonstrated a good integration of the grafts in the host tissue, showing the presence of a thin fibrotic cellular overgrowth around the implant (Fig. 2 B). The fibrotic capsule was characterized by the presence of fibroblasts as shown by immunofluorescence analyses of explanted grafts (Fig. 2C).; however, host cells were able to overcome the fibrotic capsule and homogeneously colonize the ES-SF samples (Fig. 2 B).

Immunofluorescence analyses of explanted grafts showed a low inflammatory response (Fig. 2 D). Few inflammatory macrophages, stained with anti-ED1 antibody, were observed in the fibrotic capsule and in ES-SF 4.5 ID tubular scaffolds retrieved from the animals, indicating a low inflammatory reaction (Fig. 2 D). Furthermore, T lymphocytes, stained with anti-CD4 antibody, were completely absent, demonstrating no immune reaction caused by the implanted samples from ES-SF 4.5 ID tubes (Fig. 2 D).

4. Discussion

The use of a scaffold that mimics the native structure of the ECM plays a fundamental role in tissue regeneration. For this reason, in the present study, tubular scaffolds of SF were

Microsoft Office User 15/6/21 13:42
Formattato: Inglese (Regno Unito)

obtained by electrospinning, thus combining the typical morphological properties of electrospun mats with the good biocompatibility, excellent mechanical properties and versatile processability of SF. Furthermore, ES-SF tubular scaffolds with 1.5 mm ID were produced for the first time by electrospinning of SF alone, and characterized for a possible application as small diameter graft to be used in pediatrics and in hand microsurgery. In our previous work [36], *in vivo* functionality tests of acellular ES-SF 1.5 ID tubes implanted in the abdominal aorta of Lewis rats for 7 days showed no signs of acute thrombosis and occlusion, and the absence of aneurismal dilatation and apparent intimal hyperplasia. Even after a short period of implantation, ES-SF 1.5 ID tubular scaffolds allowed the regeneration of neo-tissue similar to the native blood vessels; in fact histological and immunofluorescence analysis detected the presence of SMCs, endothelial cells (ECs), elastin and blood capillaries [36]. ES-SF tubular scaffolds induced elastin regeneration, observed only with few other tissue engineered vascular grafts [2]. In contrast, previous experiments performed by other research groups with different SF scaffold forms (i.e. gel spun tubes [5], woven thread tubes [22] and knitted tubes [23]), did not show elastin deposition in the graft lumen. The reason for the favorable results obtained with our ES-SF tubular scaffold can be attributed to the combination of the excellent biocompatibility and mechanical properties of SF and the nanostructured morphology obtained by electrospinning.

The ES-SF 4.5 ID and ES-SF 1.5 ID tubular scaffolds are made of nanofibers with a homogeneous random fiber distribution. The average diameters of electrospun SF fibers obtained from SF dissolved in formic acid can be highly variable from ~ 50 nm to ~ 1200 nm (Table 2). This variability in the fiber size may be induced by the different procedures used for SF regeneration (Table 2). Matsumoto et al. [37] demonstrated that the use of different solvents for SF solubilization may lead to different properties of SF solutions, such as the intrinsic viscosity that is related to the molecular weight. Therefore, the different procedures used for SF regeneration may cause changes in SF molecular weight. As shown in Table 2, in several works the degumming process was performed for longer time (30 min and 1 h) than in this study (15 min) and the SF solubilisation was carried out at higher temperatures (70, 85 and 100°C) using different solvents ($CaCl_2/CH_3CH_2OH$ and $CaCl_2$/ethanol instead of LiBr). Specifically, it is actually known that an increase of the degumming time causes a decrease in the SF molecular weight [14]. In general, the decrease of the molecular weight brings to a decrease of the electrospun fiber size [38-40]. The SF solubilization process used in this study seems to allow the regeneration of SF with higher molecular weight, probably resulting

in a less SF degradation during the solubilization process and the correspondent major maintenance of the properties of the raw SF.

Table 2. Diameter values of electrospun fibers related to degumming and solubilization processes.

Degumming	Solubilization	Fiber diameter	Ref.
0.5% (w/w) $NaHCO_3$ solution at 100 °C for 30 min (twice)	$CaCl_2/CH_3CH_2OH/H_2O$ (1:2:8 in molar ratio) at 70 °C for 6 h	80 nm *	[41, 42]
		150 to 300 nm [a]	[43]
aqueous solution of 0.3% marseillus soap and 0.2% Na_2CO_3, at 100 °C for 1 h	$CaCl_2/H_2O$/ethanol (1:8:2 in molar ratio) at 85 °C for 3 min	265 nm *	[44]
0.02 M aqueous Na_2CO_3 at 100 °C for 30 min	50% aqueous $CaCl_2$ at 100 °C	56 nm * 65 nm *	[45]
2 g/L Na_2CO_3 solution and 1 g/L anionic detergent at 100 °C for 1 h	$CaCl_2/CH_3CH_2OH/H_2O$ (1:2:8 in molar ratio) at 70 °C for 4 h	85.5 nm * 165.3 nm * 206.8 nm *	[46]
0.5% (w/w) Na_2CO_3 aqueous solutions for 30 min (twice)	9.3 M LiBr solution at 60 °C	400 nm * 800 nm * 1200 nm *	[47]
autoclave at 120 °C for 15 min	9.3 M LiBr solution at 60 °C for 3 h	750 nm *	[25]
autoclave at 120 °C for 15 min	9.3 M LiBr solution at 60 °C for 3 h	550 nm *	this study

* average value, [a] range from the minimum to the maximum diameter

SEM observations showed a random fiber distribution, as the tubular scaffolds were fabricated with a collector rotation rate of ~ 2700 rpm, corresponding to a collector tangential speed (~ 0.65 m/s and ~ 0.20 m/s for ES-SF 4.5 ID and ES-SF 1.5 ID, respectively), too low to allow for circumferential fibers alignment. To obtain fiber alignment in a circumferential manner onto the cylinder surface, the tangential speed has to exceed the fiber delivery rate (tangential speed ≥ 2-2.5 m/s [48, 49]). However, the random nanofiber distribution of ES-SF

1.5 ID tubes showed an appropriate morphology for a good interaction with primary porcine SMCs and for the regeneration of vessel-like structure [36].

Concerning the mechanical properties, only ES-SF 4.5 ID tubular scaffolds showed significantly higher ultimate tensile strength (UTS) and lower strain at break obtained by circumferential tensile tests than those measured by axial tensile tests, indicating anisotropic properties of the scaffolds. The anisotropic mechanical behavior may be related to a slight different fiber orientation in the tube wall. In comparison to ES-SF 1.5 ID tubular scaffolds, the anisotropic behavior of ES-SF 4.5 ID tubes may be affected by different collector tangential speed (~ 0.65 m/s and ~ 0.20 m/s for ES-SF 4.5 ID and ES-SF 1.5 ID, respectively) and electric field, due to the different collector diameter.

Substitutes for blood vessel regeneration must demonstrate adequate mechanical properties. ES-SF tubular scaffolds are here compared with electrospun scaffolds made of a synthetic polymer, PCL, that is widely used for vascular tissue engineering applications, and a natural polymer, elastin, that is one of the major ECM proteins in the arterial wall. ES-SF tubes exhibited higher UTS and strain at break than electrospun tropoelastin scaffolds, but lower than electrospun PCL scaffolds (Table 3). This comparison demonstrated that ES-SF tubular scaffolds showed higher mechanical than another natural polymer, but lower than a synthetic polymer. Specifically, ES-SF tubes showed higher elongation than elastin, that usually exhibits great elongation. ES-SF tubes showed a higher UTS in circumferential direction than native anterior descending human coronary arteries and higher strain at break than human saphenous veins, the gold standard for arterial by-pass grafts, in both directions (Table 3). Therefore, ES-SF tubes demonstrated appropriate tensile mechanical properties for small diameter blood vessel regeneration.

Table 3. Mechanical properties of ES-SF tubular scaffold, other electrospun scaffolds and native blood vessels.

Graft	UTS [MPa]	ε_b [%]	Reference
ES-SF 4.5 ID	1.24 ± 0.06 [c] 0.83 ± 0.13 [a]	141 ± 19 [c] 224 ± 29 [a]	this study
ES-SF 1.5 ID	0.90 ± 0.07 [c] 0.95 ± 0.09 [a]	210 ± 33 [c] 199 ± 16 [a]	this study
electrospun tropoelastin	0.34 ± 0.14 [c] 0.38 ± 0.05 [a]	79 ± 6 [c] 75 ± 5 [a]	[11]
electrospun PCL	4.0 ± 0.4 [a]	140 ± 13 [a]	[50]
	4.1 ± 0.5 [a]	1092 ± 28 [a]	[10]
human coronary artery	0.39 ± 0.07 [c]	-	[51]
human saphenous vein	3.01 ± 1.91 [c] 13.22 ± 5.73 [a]	11 ± 5 [c] 17 ± 10 [a]	[52]

[c]: circumferential, [a]: axial

Due to the permeability of the ES-SF tubes at pressures higher than 80 mmHg [25], in a previous work [25] a highly deformable balloon was inflated inside the sample under a controlled pressure for the measurement of the compliance and the burst pressure, in accordance with the ISO 7198. Considering the very small internal diameter of the ES-SF 1.5 ID scaffolds, it was impossible to experimentally measure their compliance and burst pressure, since no balloon with the adequate properties was commercially available. For this reason, in this work the burst pressure and distensibility of ES-SF tubular scaffolds were theoretically estimated. The distensibility coefficient can be used also as a preliminary estimation of the ES-SF tubular scaffold compliance. The DC of native rat aorta was significantly higher than that of Goretex® prosthesis ($p < 0.05$), as previously reported [3]. The DC of ES-SF 1.5 ID tubular scaffolds was significantly higher than that of Goretex® prosthesis and native rat aorta ($p < 0.05$), demonstrating an adequate behavior for blood vessel regeneration. Specifically, the DC of ES-SF 1.5 ID tubes and native rat aorta was equal to 0.58 ± 0.03 %/100 mmHg and 0.32 ± 0.04 %/100 mmHg, respectively. However, the used

method underestimates the DC of native rat aorta, since the rat aorta is not a thin-walled hollow cylinder; in fact the ratio between the thickness and the diameter is equal to 0.126, which is slightly higher than the reference value (0.1 [53]). ES-SF 4.5 ID tubular scaffolds exhibited similar DC (0.20 ± 0.01 %/100 mmHg) to native rat aorta and Goretex® prosthesis ($p > 0.05$), but significantly lower than ES-SF 1.5 ID tubes ($p < 0.05$). The different DC between ES-SF 4.5 ID and ES-SF 1.5 ID tubes may be related to a slight different fiber orientation in the scaffold wall. The burst pressure of the two different ID tubes was estimated and it is comparable with the burst pressure of electrospun SF tubes, experimentally measured in other studies as 811 mmHg and 575 mmHg, respectively [24, 25]. These studies used different solutions for SF electrospinning (an aqueous blend of SF and PEO [24] and a solution of SF and formic acid [25]) and different systems for measuring the burst pressure, that could be the causes of the different burst pressure values reported. Furthermore, the ES-SF tubes developed in this study bore up to a pressure value higher than the upper pathological pressures (180 – 220 mmHg), but lower than native human saphenous veins (~ 2,000 mmHg [54]). However, preliminary in vivo functionality tests showed no mechanical issues of the ES-SF grafts [36]. Furthermore, ES-SF grafts showed a fast regeneration of the vessel-like structure [36] that may allow the support of in vivo mechanical loading.

The suture retention strength (SRS) value of the thickest ES-SF 1.5 ID tubular scaffolds (wall thickness = 120 ± 25 μm) was appropriate for the specific application, in fact the value was similar to that of native internal mammary artery (0.76 – 2.01 N [55]). Furthermore, the SRS values of ES-SF 1.5 ID tubes (wall thickness = 80 ± 15 μm and 120 ± 25 μm) were higher than those of other natural polymer-based scaffolds, such as fibrin gel. Fibrin gels with embedded cells exhibited a SRS value equal to 0.19 ± 0.05 N, that were obtained by applying a lower crosshead displacement rate (2 mm/min) [12] than the value range indicated in the ISO 7198. Although fibrin gels were *in vitro* conditioned to enhance the cells alignment, the SRS of fibrin gels was lower than that of ES-SF tubes. Electrospun PCL tubes exhibited higher SRS values (4.8 – 9.18 N [9, 10]) than those of ES-SF 1.5 ID. However, the SRS values of ES-SF 1.5 ID (wall thickness = 80 ± 15 μm) are similar to that of PGS porous tubes coating with electrospun PCL (0.45 ± 0.031 N applying a crosshead displacement rate of 2 mm/min [8]). PGS-PCL scaffolds showed an excellent biological behavior as interposition grafts in rat abdominal aorta for 3 months [8], demonstrating an appropriate SRS value during the *in vivo* model. Therefore, also the SRS of ES-SF 1.5 ID tubular scaffolds (wall

thickness = 80 ± 15 μm) should be appropriate for the *in vivo* characterization, as demonstrated by the *in vivo* implantation in the rat model for 7 days [36].

ES-SF tubes displayed a degradation kinetic similar to other regenerated SF materials, like films (weight loss = 45.5%, after 17 days) [56], with a rate significantly higher than that of natural SF fibers (weight loss ~ 7% [32] or ~ 2% [56], after 17 days), probably due to the higher surface exposed to the enzyme in the ES-SF scaffolds. The increase of the crystallinity index value at short incubation time can be attributed to the quenching effect of the water treatment on SF chains which attained a more ordered crystalline structure on wetting and subsequent drying. By increasing the exposition time to protease, the external SF layers underwent a decrease of order and crystallinity, as demonstrated by FTIR and SEM analysis. As a consequence of the protease activity, the nanofibers were attacked from the outside; in fact DSC analysis showed an increase of the crystallinity of the bulk ES-SF tubes due to the digestion and a decrease of amorphous regions, confirming the surface degradation of the ES-SF tubes. Zhou et al. [26] studied the degradation behavior of aqueous-derived electrospun SF tubes using Protease XIV. About 65% of the electrospun SF scaffolds was degraded within 24 days in the enzymatic solution [26] with an enzyme/substrate ratio equal to 0.06 U/mg, demonstrating a faster degradation kinetics than ES-SF tubes developed in this study that showed a weight loss of ~ 35% after 24 days with an enzyme/substrate ratio equal to 0.1 U/mg. Probably, the degradation behavior of our ES-SF scaffolds compared to the Zhou's work may be correlated to the SF regeneration procedure, specifically Zhou's electrospun SF tubes were fabricated following an all-aqueous process. In fact, Wang et al. [57] demonstrated that *in vivo* degradation kinetic of aqueous-derived SF scaffolds was faster than HFIP-derived SF scaffolds.

The *in vitro* cytocompatibility of ES-SF tubes was confirmed by the adhesion and growth of SMCs onto the ES-SF 1.5 ID tubular scaffolds. In some cases, the porosity of electrospun scaffolds may limit or not allow the cell infiltration inside the scaffold [16, 58]. ES-SF 1.5 ID tubes, seeded using a rotational method, exhibited a homogenous cell distribution onto the external surface and a heterogeneous distribution in the tube wall thickness. Furthermore, SMCs, seeded on the external surface, were able to migrate in the ES-SF 1.5 ID tube wall thickness, reaching the lumen.

In vivo subcutaneous implants showed the presence of few macrophages, demonstrating a low physiological inflammatory reaction of the recipient to the subcutaneously implanted material at 15 days after implantation, demonstrating the complete evaporation of formic acid, the toxic solvent used for electrospinning. The absence of T lymphocytes demonstrated

no cell-mediated immunoresponse. As expected, these data confirm the good *in vivo* biocompatibility of SF scaffolds; actually, SF is widely used for tissue engineering applications. At 15 days after implantation, the H&E analysis exhibited the formation of a thin fibrotic capsule mainly populated by fibroblasts, suggesting the completion of the host response to the implant. As shown by H&E analysis and macroscopic evaluation of explanted ES-SF tubes (data not reported), ES-SF tubes remained stable with shape maintenance in a subcutaneous environment for 15 days.

5. Conclusions

Nanostructured tubular scaffolds with inner diameter of 4.5 mm and 1.5 mm were successfully fabricated by electrospinning a solution of SF in formic acid. The *in vitro* characterization of the ES-SF tubular scaffolds performed in this study provided promising results in terms of morphological, mechanical, biological and biodegradation behavior for their possible use as off-the-shelf scaffolds for the regeneration of small diameter blood vessels. Specifically, ES-SF tubular scaffolds showed a random fiber distribution in the nanometric range, allowing for the *in vitro* adhesion and growth of primary porcine SMCs. The ES-SF 1.5 ID morphological characteristic was appropriate for cell migration, indeed SMCs seeded on the external surface were able to migrate through the wall thickness, reaching the lumen. ES-SF tubular scaffolds exhibited an appropriate mechanical performance, in terms of axial and circumferential tensile properties, suture retention strength, burst pressure and distensibility. These promising results were confirmed by *in vivo* functionality tests in the abdominal aorta of Lewis rats for 7 days, performed in our previous work [36], where acellular ES-SF 1.5 ID tubular scaffolds allowed the regeneration of neo-tissue similar to the native blood vessels.

Acknowledgements

The work was supported by Cariplo Foundation funds to G. Freddi (Project No. 2007-5457). The authors would like to thank Dr. Francesco Migliavacca, Dr. Lina Altomare and Dr. Giancarlo Pennati for the useful discussion on mechanical analysis.

References

[1] A. Rathore, M. Cleary, Y. Naito, K. Rocco, C. Breuer, Wires Nanomed Nanobi, 4 (2012) 257-272.

[2] D. Pankajakshan, D.K. Agrawal, Can J Physiol Pharm, 88 (2010) 855-873.

[3] V. Catto, S. Farè, G. Freddi, M.C. Tanzi, ISRN Vascular Medicine, Volume 2014, Article ID 923030 27 pages.
[4] A. Hasan, A. Memic, N. Annabi, M. Hossain, A. Paul, M.R. Dokmeci, F. Dehghani, A. Khademhosseini, Acta Biomater, 10 (2014) 11-25.
[5] M. Lovett, G. Eng, J.A. Kluge, C. Cannizzaro, G. Vunjak-Novakovic, D.L. Kaplan, Organogenesis, 6 (2010) 217-224.
[6] A.F. Pellegata, M.A. Asnaghi, I. Stefani, A. Maestroni, S. Maestroni, T. Dominioni, S. Zonta, G. Zerbini, S. Mantero, BioMed Research International, 2013 (2013) 8.
[7] S.W. Cho, I.K. Kim, J.M. Kang, K.W. Song, H.S. Kim, C.H. Park, K.J. Yoo, B.S. Kim, Tissue Eng Part A, 15 (2009) 901-912.
[8] W. Wu, R.A. Allen, Y. Wang, Nat Med, 18 (2012) 1148-1153.
[9] S. de Valence, J.C. Tille, J.P. Giliberto, W. Mrowczynski, R. Gurny, B.H. Walpoth, M. Moller, Acta Biomater, 8 (2012) 3914-3920.
[10] S. de Valence, J.C. Tille, D. Mugnai, W. Mrowczynski, R. Gurny, M. Moller, B.H. Walpoth, Biomaterials, 33 (2012) 38-47.
[11] K.A. McKenna, M.T. Hinds, R.C. Sarao, P.C. Wu, C.L. Maslen, R.W. Glanville, D. Babcock, K.W. Gregory, Acta Biomater, 8 (2012) 225-233.
[12] Z.H. Syedain, L.A. Meier, J.W. Bjork, A. Lee, R.T. Tranquillo, Biomaterials, 32 (2011) 714-722.
[13] G.H. Altman, F. Diaz, C. Jakuba, T. Calabro, R.L. Horan, J. Chen, H. Lu, J. Richmond, D.L. Kaplan, Biomaterials, 24 (2003) 401-416.
[14] L.S. Wray, X. Hu, J. Gallego, I. Georgakoudi, F.G. Omenetto, D. Schmidt, D.L. Kaplan, J Biomed Mater Res B Appl Biomater, 99 (2011) 89-101.
[15] D.N. Rockwood, R.C. Preda, T. Yucel, X. Wang, M.L. Lovett, D.L. Kaplan, Nat Protoc, 6 (2011) 1612-1631.
[16] R.L. Dahlin, F.K. Kasper, A.G. Mikos, Tissue Eng Part B Rev, 17 (2011) 349-364.
[17] Y. Zhang, C.T. Lim, S. Ramakrishna, Z.M. Huang, J Mater Sci Mater Med, 16 (2005) 933-946.
[18] S.G. Kumbar, R. James, S.P. Nukavarapu, C.T. Laurencin, Biomed Mater, 3 (2008) 034002.
[19] F. Kuwabara, Y. Narita, A. Yamawaki-Ogata, M. Satake, H. Kaneko, H. Oshima, A. Usui, Y. Ueda, J Artif Organs, 15 (2012) 399-405.
[20] W. He, Z. Ma, W.E. Teo, Y.X. Dong, P.A. Robless, T.C. Lim, S. Ramakrishna, J Biomed Mater Res A, 90 (2009) 205-216.

[21] D. Zhang, J. Chang, Nano Lett, 8 (2008) 3283-3287.
[22] S. Enomoto, M. Sumi, K. Kajimoto, Y. Nakazawa, R. Takahashi, C. Takabayashi, T. Asakura, M. Sata, J Vasc Surg, 51 (2010) 155-164.
[23] T. Yagi, M. Sato, Y. Nakazawa, K. Tanaka, M. Sata, K. Itoh, Y. Takagi, T. Asakura, J Artif Organs, 14 (2011) 89-99.
[24] L. Soffer, X. Wang, X. Zhang, J. Kluge, L. Dorfmann, D.L. Kaplan, G. Leisk, J Biomater Sci Polym Ed, 19 (2008) 653-664.
[25] B. Marelli, A. Alessandrino, S. Fare, G. Freddi, D. Mantovani, M.C. Tanzi, Acta Biomater, 6 (2010) 4019-4026.
[26] J. Zhou, C. Cao, X. Maa, L. Hua, L. Chen, C. Wang, Polym Degrad Stabil, 95 (2010) 1679-1685.
[27] J. Zhou, C. Cao, X. Ma, Int J Biol Macromol, 45 (2009) 504-510.
[28] H. Liu, X. Li, G. Zhou, H. Fan, Y. Fan, Biomaterials, 32 (2011) 3784-3793.
[29] A.E. Terry, D.P. Knight, D. Porter, F. Vollrath, Biomacromolecules, 5 (2004) 768-772.
[30] R. Gauvin, M. Guillemette, T. Galbraith, J.M. Bourget, D. Larouche, H. Marcoux, D. Aube, C. Hayward, F.A. Auger, L. Germain, Tissue Eng Part A, 17 (2011) 2049-2059.
[31] A. Benetos, S. Laurent, A.P. Hoeks, P.H. Boutouyrie, M.E. Safar, Arterioscler Thromb, 13 (1993) 90-97.
[32] R.L. Horan, K. Antle, A.L. Collette, Y. Wang, J. Huang, J.E. Moreau, V. Volloch, D.L. Kaplan, G.H. Altman, Biomaterials, 26 (2005) 3385-3393.
[33] G. Freddi, G. Pessina, M. Tsukada, Int J Biol Macromol, 24 (1999) 251-263.
[34] C. Arrigoni, A. Chitto, S. Mantero, A. Remuzzi, Biotechnol Bioeng, 100 (2008) 988-997.
[35] A. Motta, L. Fambri, C. Migliaresi, Macromol Chem Phys, 203 (2002) 1658-1665.
[36] I. Cattaneo, M. Figliuzzi, N. Azzollini, V. Catto, S. Fare, M.C. Tanzi, A. Alessandrino, G. Freddi, A. Remuzzi, Int J Artif Organs, 36 (2013) 166-174.
[37] K. Matsumoto, H. Uejima, J Polymer Sci Polymer Chem 35 (1997) 1949-1954.
[38] Q.P. Pham, U. Sharma, A.G. Mikos, Tissue Eng, 12 (2006) 1197-1211.
[39] C. Mit-uppatham, M. Nithitanakul, P. Supaphol, Macromol Chem Phys, 205 (2004) 2327-2338.
[40] Z. Jun, H. Hou, J.H. Wendorff, A. Greiner, e-Polymers, 038 (2005).
[41] B.M. Min, G. Lee, S.H. Kim, Y.S. Nam, T.S. Lee, W.H. Park, Biomaterials, 25 (2004) 1289-1297.

[42] B.M. Min, L. Jeong, Y.S. Nam, J.M. Kim, J.Y. Kim, W.H. Park, Int J Biol Macromol, 34 (2004) 281-288.
[43] K.H. Kim, L. Jeong, H.N. Park, S.Y. Shin, W.H. Park, S.C. Lee, T.I. Kim, Y.J. Park, Y.J. Seol, Y.M. Lee, Y. Ku, I.C. Rhyu, S.B. Han, C.P. Chung, J Biotechnol, 120 (2005) 327-339.
[44] C.S. Ki, S.Y. Park, H.J. Kim, H.M. Jung, K.M. Woo, J.W. Lee, Y.H. Park, Biotechnol Lett, 30 (2008) 405-410.
[45] S. Sukigara, M. Gandhi, J. Ayutsede, M. Micklus, F. Ko, Polymer, 44 (2003) 5721–5727.
[46] N. Amiraliyan, M. Nouri, K.M. H., Polymer Science Ser A 52 (2010) 407-412.
[47] J. Qu, D. Wang, H. Wang, Y. Dong, F. Zhang, B. Zuo, H. Zhang, J Biomed Mater Res A, (2013).
[48] T. Courtney, M.S. Sacks, J. Stankus, J. Guan, W.R. Wagner, Biomaterials, 27 (2006) 3631-3638.
[49] C.H. Lee, H.J. Shin, I.H. Cho, Y.M. Kang, I.A. Kim, K.D. Park, J.W. Shin, Biomaterials, 26 (2005) 1261-1270.
[50] S.J. Lee, J. Liu, S.H. Oh, S. Soker, A. Atala, J.J. Yoo, Biomaterials, 29 (2008) 2891-2898.
[51] E. Claes, J.M. Atienza, G.V. Guinea, F.J. Rojo, J.M. Bernal, J.M. Revuelta, M. Elices, Conf Proc IEEE Eng Med Biol Soc, 2010 (2010) 3792-3795.
[52] D.L. Donovan, S.P. Schmidt, S.P. Townshend, G.O. Njus, W.V. Sharp, J Vasc Surg, 12 (1990) 531-537.
[53] J.R. Basford, Arch Phys Med Rehabil, 83 (2002) 1165-1170.
[54] M. Peck, D. Gebhart, N. Dusserre, T.N. McAllister, N. L'Heureux, Cells Tissues Organs, 195 (2012) 144-158.
[55] G. Konig, T.N. McAllister, N. Dusserre, S.A. Garrido, C. Iyican, A. Marini, A. Fiorillo, H. Avila, W. Wystrychowski, K. Zagalski, M. Maruszewski, A.L. Jones, L. Cierpka, L.M. de la Fuente, N. L'Heureux, Biomaterials, 30 (2009) 1542-1550.
[56] T. Arai, G. Freddi, R. Innocenti, M. Tsukada, J Appl Polym Sci, 91 (2004) 2383-2390.
[57] Y. Wang, D.D. Rudym, A. Walsh, L. Abrahamsen, H.J. Kim, H.S. Kim, C. Kirker-Head, D.L. Kaplan, Biomaterials, 29 (2008) 3415-3428.
[58] N. Bhardwaj, S.C. Kundu, Biotechnol Adv, 28 (2010) 325-347.